Earth and Space Science

RESEARCH ARTICLE
10.1029/2024EA003803

The Critical Role of Sea Ice Products for Accurate Wind-Wave Simulations in the Arctic

Tyler W. Miesse[1], Martin Henke[1], Andre de Souza de Lima[1], Celso M. Ferreira[1], and Thomas Ravens[2]

[1]Department of Civil, Environmental, and Infrastructure Engineering, George Mason University, Fairfax, VA, USA, [2]Department of Civil Engineering, University of Alaska Anchorage, Anchorage, AK, USA

Key Points:

- The wave model was able to accurately represent four different extreme events in the Alaskan Arctic under different sea ice conditions
- ERA5 showed the highest correlation values during all events in this study when compared to the satellite observations
- An ensemble combining all sea ice products was also evaluated and produced consistently high correlation to the observations

Supporting Information:

Supporting Information may be found in the online version of this article.

Correspondence to:

T. W. Miesse,
tmiesse@gmu.edu

Citation:

Miesse, T. W., Henke, M., de Souza de Lima, A., Ferreira, C. M., & Ravens, T. (2025). The critical role of sea ice products for accurate wind-wave simulations in the Arctic. *Earth and Space Science*, *12*, e2024EA003803. https://doi.org/10.1029/2024EA003803

Received 14 JUN 2024
Accepted 9 JAN 2025

Author Contributions:

Conceptualization: Tyler W. Miesse
Formal analysis: Tyler W. Miesse
Investigation: Andre de Souza de Lima
Methodology: Tyler W. Miesse
Supervision: Celso M. Ferreira, Thomas Ravens
Validation: Tyler W. Miesse, Martin Henke
Visualization: Tyler W. Miesse
Writing – original draft: Tyler W. Miesse
Writing – review & editing: Tyler W. Miesse, Martin Henke, Andre de Souza de Lima, Celso M. Ferreira, Thomas Ravens

Abstract The Arctic region is experiencing significant changes due to climate change, and the resulting decline in sea ice concentration and extent is already impacting ocean dynamics and exacerbating coastal hazards in the region. In this context, numerical models play a crucial role in simulating the interactions between the ocean, land, sea ice, and atmosphere, thus supporting scientific studies in the region. This research aims to evaluate how different sea ice products with spatial resolutions varying from 2 to 25 km influence a phase averaged spectral wave model results in the Alaskan Arctic under storm conditions. Four events throughout the Fall to Winter seasons in 2019 were utilized to assess the accuracy of wave simulations generated under the dynamic sea ice conditions found in the Arctic. The selected sea ice products used to parameterize the numerical wave model include the National Snow and Ice Data Center (NSIDC) sea ice concentration, the European Centre for Medium-Range Weather Forecasts (ECMWF) Re-Analysis (ERA5), the HYbrid Coordinate Ocean Model-Community Ice CodE (HYCOM-CICE) system assimilated with Navy Coupled Ocean Data Assimilation (NCODA), and the High-resolution Ice-Ocean Modeling and Assimilation System (HIOMAS). The Simulating WAves Nearshore (SWAN) model's accuracy in simulating waves using these sea ice products was evaluated against Sea State Daily Multisensor L3 satellite observations. Results show wave simulations using ERA5 consistently exhibited high correlation with observations, maintaining an accuracy above 0.83 to the observations across all events. Conversely, HIOMAS demonstrated the weakest performance, particularly during the Winter, with the lowest correlation of 0.40 to the observations. Remarkably, ERA5 surpassed all other products by up to 30% in accuracy during the selected storm events, and even when an ensemble was assessed by combining the selected sea ice products, ERA5's individual performance remained unmatched. Our study provides insights for selecting sea ice products under different sea ice conditions for accurately simulating waves and coastal hazards in high latitudes.

Plain Language Summary The Arctic is changing rapidly due to climate change, resulting in a significant decrease in sea ice. This reduction affects ocean conditions and increases coastal hazards. Our study examines how varying sea ice data resolutions, ranging from 2 to 25 km, influence the results of a wave model during four storm events in the Alaskan Arctic from Fall to Winter 2019. We incorporated sea ice data into our wave model from various sources: the National Snow and Ice Data Center (NSIDC), the European Centre for Medium-Range Weather Forecasts (ECMWF, known as ERA5), the HYbrid Coordinate Ocean Model-Community Ice CodE (HYCOM-CICE) system, and the High-resolution Ice-Ocean Modeling and Assimilation System (HIOMAS). We then evaluated the accuracy of wave forecasts produced by the Simulating Waves Nearshore (SWAN) model by comparing them with satellite observations. Our findings indicate that the ERA5 data provided the most accurate wave predictions, demonstrating a high correlation (above 0.83) with satellite observations during all storm events. Conversely, the HIOMAS data showed the weakest results relative to the other products, particularly in Winter, with the lowest correlation (0.40) and higher errors. Notably, ERA5 outperformed the other products by up to 30% in accuracy during the storms, and even when combining different sea ice data, ERA5's performance remained superior. This study offers valuable insights into selecting sea ice data for accurately predicting waves and coastal hazards in the Arctic. These findings are crucial for understanding and preparing for the impacts of climate change in this vulnerable region.

1. Introduction

The Arctic region has undergoing significant changes due to climate change (Hartmuth et al., 2023; Serreze et al., 2000) leading to reduced sea ice presence and increased coastal hazards (Forbes & Taylor, 1994; Hume &

Schalk, 1967; Short & Wiseman, 1974; Urdea, 2007). The warmer climate is creating longer open water seasons in the Arctic Ocean, producing larger fetches and enabling the growth of larger wind waves (Overeem et al., 2011; Waseda et al., 2018). The reduction in sea ice has also led to changes in the ocean currents, atmospheric circulation, and the cryosphere, which have a cascading effect on the ecosystems and human activities (Valkonen et al., 2021).

To better understand the impacts of sea ice decline in the Arctic coastal regions, ocean and coastal models have become essential tools (Kousal et al., 2022; Thomson & Rogers, 2014; D. M. Williams & Erikson, 2021). These models simulate the behavior of waves, tides, and currents—allowing assessment of the effects of storms, sea level rise, and other coastal hazards (Dietrich et al., 2012; Westerink et al., 1992). Coastal modeling can also help to identify the vulnerabilities of Arctic coastal communities and infrastructure to changing environmental conditions (Squire, 2018; D. M. Williams & Erikson, 2021). Additionally, wave and sea ice modeling in the Arctic has advanced with a multitude of methods that account for the type of sea ice and location (Squire, 2020). Wave-ice dynamic interactions are important processes in the Arctic, not only for the breaking of ice floes and the melting of ice, but also for wave generation, propagation, and dissipation in the Arctic basin, the Marginal Ice Zone (MIZ), and coastal regions (Squire & Williams, 2008; T. D. Williams et al., 2013). The interaction between waves and sea ice depends on the concentration, thickness, and distribution of the ice, as well as the characteristics of the waves, such as their frequency and direction (Rogers, 2019). The wave-ice interaction schemes added to the wave models can be separated into two categories: scattering modules (IS), and dissipation modules (IC). The advancements to the wave models using these schemes have been implemented in WaveWatch III (Collins & Rogers, 2017) and the Simulating WAves Nearshore model (SWAN, Rogers, 2019; The SWAN team, 2019), a widely used numerical model for simulating wind-generated waves in the ocean and nearshore coastal zones (Cassalho et al., 2022; Henke et al., 2024; Hošeková et al., 2020; Kumar et al., 2020; Yu et al., 2022).

In order to study the effects of wave dynamics on coastal hazards in the Arctic Regions, it is necessary to include spatial and temporal sea ice data from either observations or data assimilated numerical models. Satellite sea ice observations date back as far as 1978 (Cavalieri et al., 1996) providing researchers with both sea ice extent and concentration (Collard et al., 2022; Comiso & Nishio, 2008; Liu et al., 2022), while numerical models assimilate satellite observations to increase accuracy in predicting sea-ice extent and concentration (Barton et al., 2021; Posey & Preller, 1997). For instance, the National Snow Ice Data Center (NSIDC) provides sea ice concentration based on the Advanced Microwave Scanning Radiometer (AMSR-E), Special Scanning Microwave Imager (SSM/I), and the Scanning Multichannel Microwave Radiometer (SMMR) sensors aboard the EOS-Aqua satellite (Comiso & Nishio, 2008). The European Centre for Medium-Range Weather Forecasts (ECMWF) Re-Analysis (ERA5) produces sea ice concentration through ensemble data assimilation of the reanalysis of two data sets from the Ocean and Sea Ice Satellite Application Facilities (OSI-SAF) (Hirahara et al., 2016). The two-way coupled ocean and sea ice model HYbrid Coordinate Ocean Model (HYCOM) and the Los Alamos National Laboratory Community Ice CodE (CICE), which is assimilated with Navy Coupled Ocean Data Assimilation (NCODA) system, provides high-accuracy predictions of the sea ice and ocean dynamics in the Arctic (Posey et al., 2010). Finally, the High-resolution Ice-Ocean Modeling and Assimilation System (HIOMAS) is a sea ice-ocean model that is forced with daily reanalysis of atmospheric characteristics from NCEP/NCAR (Zhang, 2021). The sea ice models differ in spatial and temporal representations of the sea ice along with varying uncertainty and accuracy (Hersbach et al., 2020; Hirahara et al., 2016; Lindsay & Schweiger, 2015). Overall, continued development and improvement of sea ice models is critical for advancing our understanding of Arctic Sea ice dynamics and their impacts on the coastal regions.

In this context, this study aims to evaluate how different sea ice products, with spatial resolutions varying from 2 to 25 km and different predicted sea-ice extents, can influence the accuracy of simulations of wave generation, propagation, and dissipation in the Alaskan Arctic under extreme meteorological conditions. Four storm events that occurred in the Fall of 2019 were used to assess the accuracy of simulating waves under various sea ice conditions along the northern coast of Alaska, the Chukchi Sea, and the Beaufort Sea. This study focuses on the freezing season, where sea ice formation and expansion dominate the wave-ice interaction dynamics. First, the wave model was validated with the Sea State Daily Multisensor L3 satellite data under ice-free conditions. Subsequently, the validated modeling framework was applied to the remaining events—which occurred under varying sea-ice conditions across different seasons. The model performance was assessed as a function of the satellite observations to highlight the overall impact the changing sea ice has on the wave model. Next, we pursued a qualitative analysis of the implications of varying spatial and temporal resolutions of sea ice products on

10.1029/2024EA003803

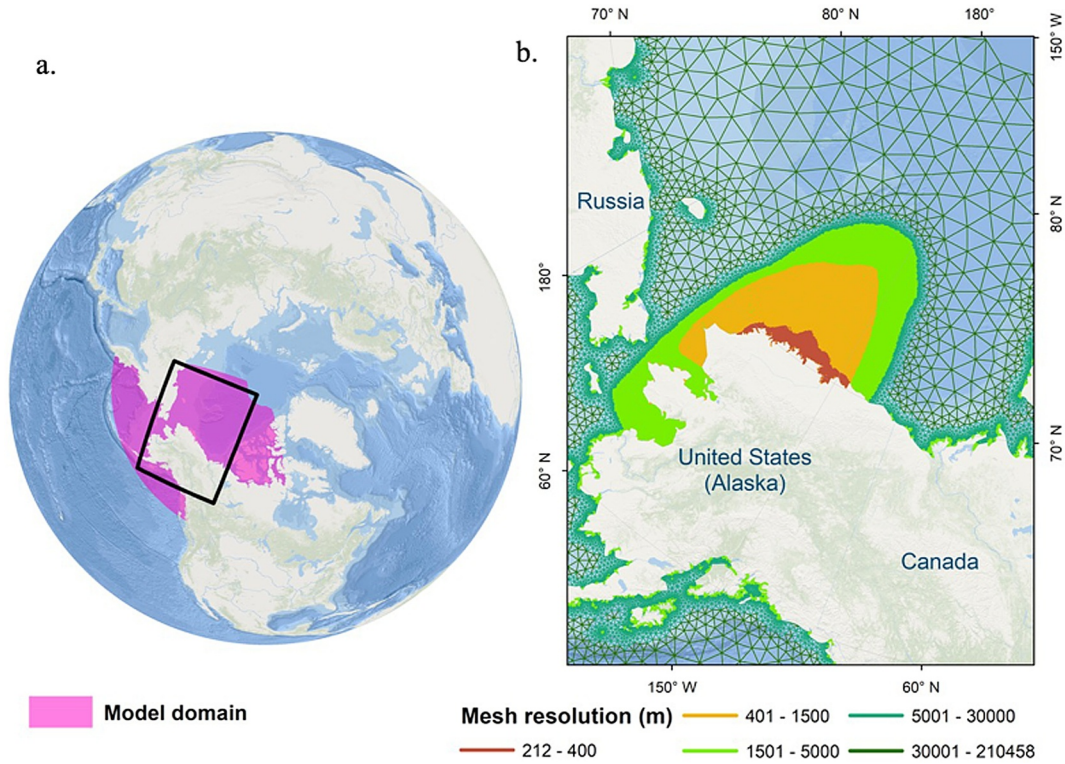

Figure 1. (a) Domain of the numerical model. (b) Focus areas of this study showing the varying resolution.

wave modeling, where key areas of influence wave dissipation were identified within the model domain. Finally, we conducted an ensemble comparison of the model results parameterized by each sea ice product to highlight the spatial disparities (i.e., areas where individual products diverge from the average) that different sea ice products can impose in wave modeling. This indicated the practicality of incorporating sea ice products into wave modeling and evaluating potential hazards for the Arctic coastal communities.

2. Methodology

2.1. Numerical Model

This study applied the coupled Advanced CIRCulation model (ADCIRC) and SWAN to simulate water levels by solving the generalized wave continuity equation (GWCE) and currents by using the vertically integrated shallow water equation (Westerink et al., 1994) with the wave model incorporating a Eulerian, phase-averaged, refraction model (Booij et al., 1999), which provides wave propagation in irregular bathymetry and topography (Gorrell et al., 2011). While water levels and currents from ADCIRC are not analyzed in this study, their representation in the modeling framework enhances the representation of the predicted waves in SWAN by solving the depth-momentum equations with the surface winds, currents, and water levels (Cassalho et al., 2022).

The ADCIRC + SWAN numerical mesh that was employed in this study extends from 55°N to its northern border at 88°N, while its longitudinal coverage extends from 160°E in Russia to 80°W in Northern Canada (Figure 1a). This unstructured grid was developed using OceanMesh2D, a MATLAB-based software for two-dimensional mesh generation (Roberts et al., 2019), which integrated varying bathymetry and topography data sources. This method followed a similar method to Joyce et al. (2019) and it allowed the numerical mesh to have a varying resolution from an average of 1.2° in the open ocean (~135 km) to 0.005° (~315 m) at the northern coast of Alaska (Figure 1c). The bathymetry and topography data were assembled from the General Bathymetric Chart of the Oceans (GEBCO) (Weatherall et al., 2015), National Oceanic and Atmospheric Administration (NOAA) Coastal Relief Model (Blanton et al., 2011), and United States Geological Survey (USGS) Coastal National Elevation Database (Danielson et al., 2016). The topography and bathymetry data was transformed based on NOAA's vertical datum transformation tool (Parker et al., 2003) to Local Mean Sea Level (LMSL). Additionally,

Table 1
Ice Products

Sea ice product	Spatial resolution	Temporal resolution
NSIDC	25 km	Daily
ERA5	0.25° ~ 32 km	Daily
HYCOM	$\frac{1}{12}$° ~ 10 km	Daily
HIOMAS	2 km	Daily

the model utilized a varying bottom friction based on the National Land Cover Database (NLCD) 2019 (Dewitz, 2021), as Manning's n coefficients (values were determined on past studies (Cassalho et al., 2022; Ferreira et al., 2014; Miesse et al., 2023; Passeri et al., 2012)), to calculate the bottom shear stress.

Advancements in the phase averaged SWAN model have allowed for sea ice and wave interaction from deep water to nearshore through an additional dissipation source term, D_{ice} (Rogers, 2019). This method of sea ice interaction follows the process developed in WaveWatch III (Collins & Rogers, 2017), and was established as IC4M2, where the temporal exponential decay rate of energy can be derived as:

$$D_{\text{ice}} = \frac{S_{\text{ice}}}{E} = -2c_g k_i \tag{1}$$

where D_{ice} is the wave dissipation term, S_{ice} is the additional sea ice source term, E is the wave energy spectrum, c_g is the group velocity, and k_i is the linear exponential attenuation rate of wave amplitude. Additionally, S_{ice} and E vary with frequency and direction. In the SWAN implementation of IC4M2, Rogers (2019) has k_i vary with frequency and can be denoted as:

$$k_i = c_0 + c_1 f + c_2 f^2 + c_3 f^3 + c_4 f^4 + c_5 f^5 + c_6 f^6 \tag{2}$$

where c_n is the user defined polynomial coefficients, and f is the frequency measured in Hz. In previous studies where this method was used in SWAN, c_2 and c_4 were the only modified coefficients while the remaining were set to zero. The c_2 and c_4 coefficients were modified in this study following the field observation study conducted in Hošeková et al. (2020), where $c_2 = 3.8 * 10^{-2}$ and $c_4 = 7.8 * 10^{-2}$. Regarding the sea ice parameterization in our model setup, we considered the findings of Branch et al. (2021), who evaluated different sea ice coefficients and highlighted that larger coefficients lead to overestimation in the wave damping. This led us to select the near ice edge coefficients, as they fall between the lower coefficients derived by Meylan et al. (2014) and the larger coefficients by Hošeková et al. (2020), which were intended for sea ice located more than 500 m from the ice edge.

2.2. Ice Products

Table 1 describes the sea ice products selected for this study, which were chosen based on different spatial/temporal resolution. Furthermore, a comparison of the sea ice concentration for each event outlined in this study is presented in Figure 2. The National Snow and Ice Datacenter (NSIDC) provides sea ice concentration (shown in Figures 2a, 2e, 2i, and 2m) from the climate data record (CDR) provided by the Defense Meteorological Satellite Program. This sea ice concentration is generated through a combination of the brightness and temperature collected from the Nimbus-7 Scanning Multichannel Microwave Radiometer, the Special Sensor Microwave Imager, and the Special Sensor Microwave Imager and Sounder (Comiso & Nishio, 2008). The algorithms developed at the NASA Goddard Space Flight Center transform the sea ice concentration into gridded data with a resolution of 25 × 25 km on the NSIDC polar stereographic grid. The European Centre for Medium-Range Weather Forecasts (ECMWF) Re-Analysis (ERA5) produces sea ice concentration through reanalysis of two OSI-SAF (Eastwood et al., 2014) products that are interpolated to the ERA5 horizontal grid (shown in Figures 2b, 2f, 2j, and 2n). Hirahara et al. (2016) discusses the uncertainties of varying data sets to enhance the reanalysis and concludes that ERA5 will include the data as a combination of the OSI-SAF products and the OSTIA sea ice (Donlon et al., 2012). The third product (Figures 2c, 2g, 2k, and 2o) is a coupled ocean and sea ice model known as HYCOM-CICE (shown only as HYCOM henceforth), which was introduced by the Naval Research Lab (Posey et al., 2010). The HYbrid Coordinate Ocean Model (HYCOM) (Metzger et al., 2008) simulates the ocean stresses, temperature, and salinity. Subsequently, it exchanges the ocean variables with the Los Alamos National Laboratory Community Ice CodE (CICE) (Hunke & Lipscomb, 2010), then CICE provides HYCOM with the sea ice physical features and flows. The framework described also incorporates data assimilation, such as the two products noted earlier, where the model is initialized with daily special sensor microwave/imager ice concentration. The last product (Figures 2d, 2h, 2l, and 2p) evaluated as a forcing in this study is the High-resolution Ice-

10.1029/2024EA003803

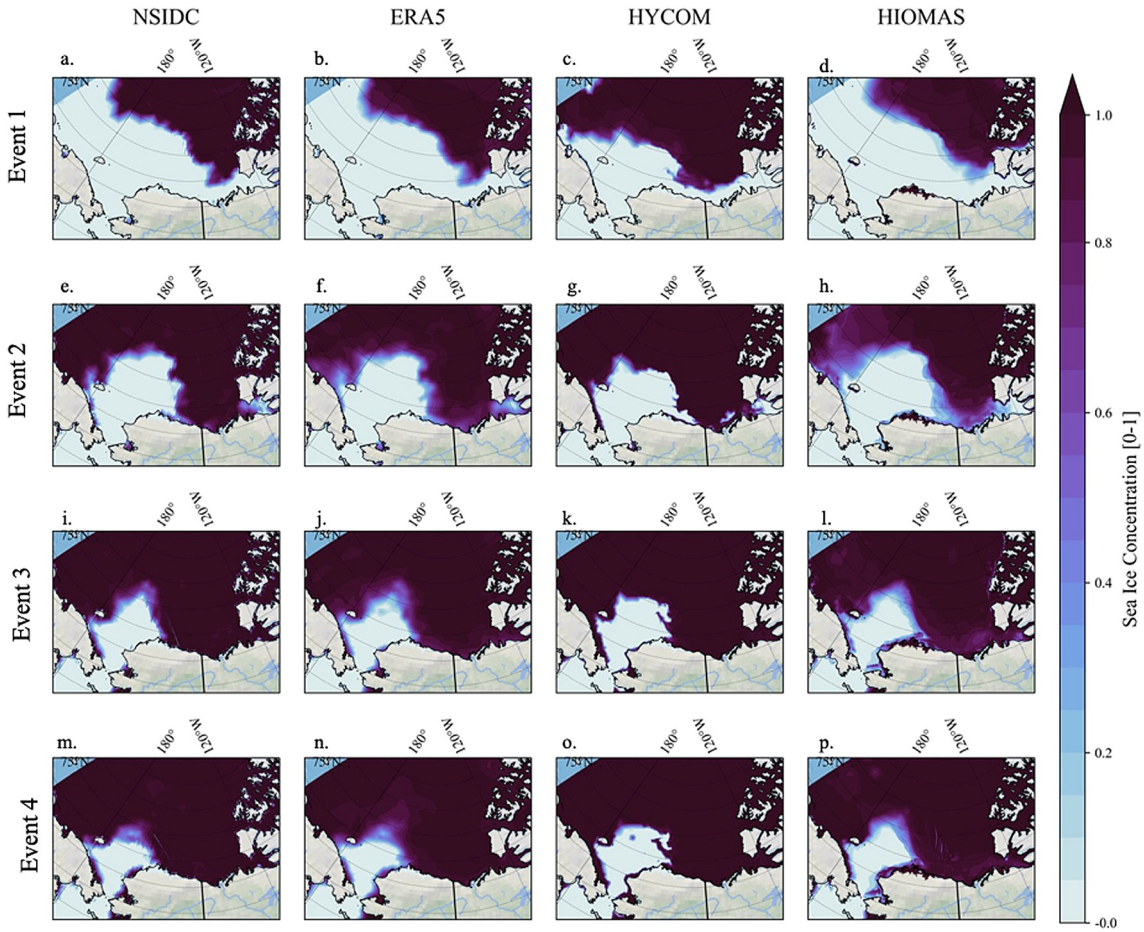

Figure 2. Sea Ice Concentration from the Sea Ice Products that was outputted from the numerical model for the four events in this study.

Ocean Modeling and Assimilation System (HIOMAS) (Zhang, 2021). This model was developed based on another sea ice model in the pan-arctic (PIOMAS), but it includes higher resolution and has the ability to assimilate satellite ice concentration like the other products discussed earlier implement. The sea ice products were compared to the ensemble average of the products to show the differences of the sea ice concentration and extents in Figure S1 in Supporting Information S1. This shows that near the marginal ice zone (MIZ), that is defined as sea ice concentration from 10% to 100%, shows the majority of the differences between the products.

2.3. Extreme Events

The Arctic experiences several types of coastal hazards (e.g., high waves, erosion and flooding) and these hazards have been increasing in intensity and frequency due to rapid environmental warming and consequent sea ice coverage reduction (Waseda et al., 2021). Table 2, shows the four events that occurred from October to December 2019 that generated waves that impacted the north slope of Alaska (Figure 3). The event in October 2019 was reported to be a mid-intensity event reported by Cassalho et al. (2022) and Yang et al. (2024). The other events were observed by Hošeková et al. (2020) showing the events generated waves along the coast. Additionally, Buzard et al. (2024) discuss how the majority of the storm events that occur from September to November in the region where the characteristics of the meteorological events in this study align with Finocchio et al. (2020). These events are introduced into the model using ERA5 winds and pressure fields at 0.25° resolution at 1 hr intervals following the results from Cassalho et al. (2022). The storms events can be classified into two types of events: arctic polar low cyclones, and arctic polar high cyclones. The first has been

Table 2
Meteorological Events From October 2019 to December 2019

Event	Type	Time of peak
Event 1	Low pressure wind event	15 October 2019
Event 2	Arctic Polar High Cyclone	12 November 2019
Event 3	Arctic Polar Low Cyclone	23 November 2019
Event 4	Arctic Polar High Cyclone	8 December 2019

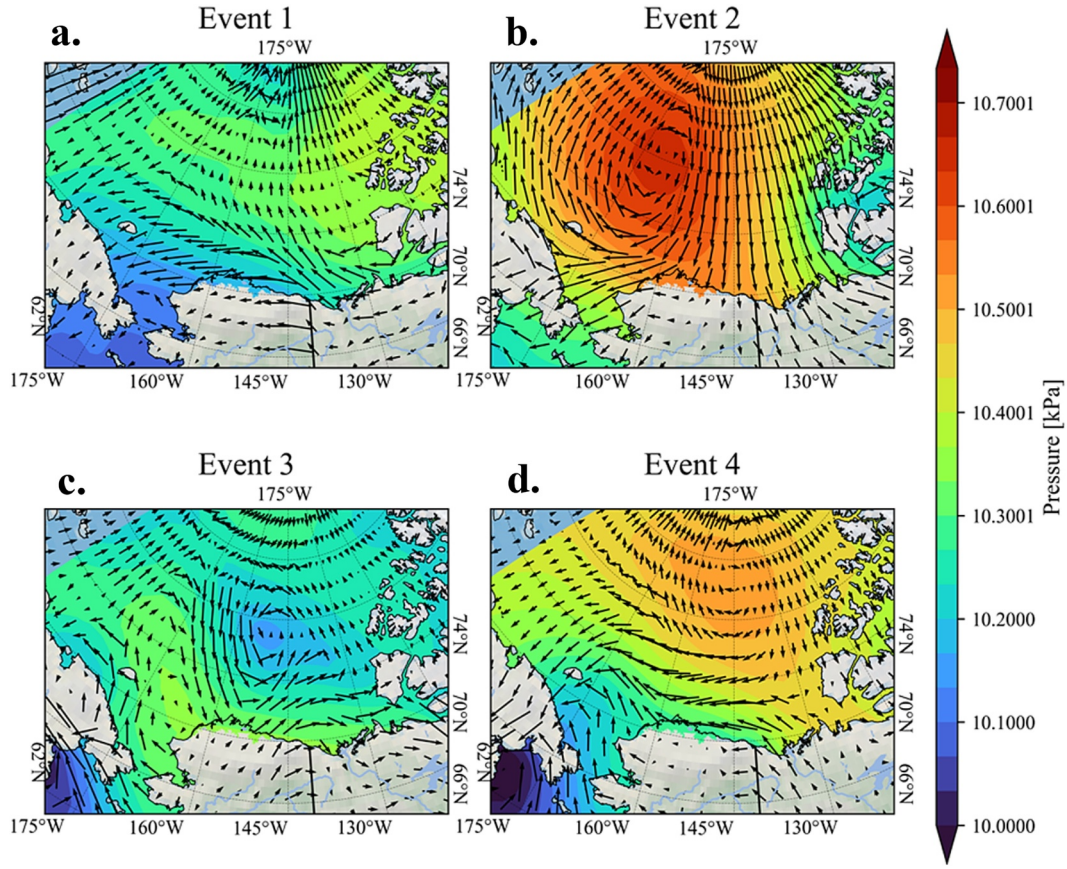

Figure 3. Meteorological Events are the pressure contours and wind vectors from ERA5 in the Arctic in Fall 2019 that is used to force the ADCIRC-SWAN model. (a) Event 1: wind event. (b) Event 2: polar high cyclone. (c) Event 3: polar low cyclone. (d) Event 4: polar high cyclone.

the subject of numerous studies and correlations have been found between declining sea ice and increasing intensity of the cyclones found in the Arctic (Valkonen et al., 2021). The Arctic Polar High cyclones (also known as anticyclonic Beaufort High) are high pressure events that occur in the Arctic Ocean with varying intensities that are correlated to other atmospheric events, such as the Icelandic low, and studies are still determining the cause/effect relationships of these cyclones (Kenigson & Timmermans, 2021; Serreze & Barrett, 2011).

First considering a polar low, in October 2019 henceforth know as Event 1, which generated an easterly wind with recorded wind speeds as high as 21.8 m/s at the NOAA Prudhoe Bay station, Alaska station, and pressures ranging as high as 10.2 kPa (shown in Figure 3a). The winds were sustained from October 15th to October 20th generating fetch limited waves that reached 3.5 m near Jones Island and up to 6.0 m in the open ocean (within 50 km of the Alaskan coast). The second polar low, known as Event 3, that we considered was a low-pressure cyclone that came from the North Pacific Ocean and followed the Bering Sea toward the Chukchi Sea on 26 November 2019 (shown Figure 3c). The cyclone continued northward to the Arctic Ocean on 28 November 2019 with pressures reaching as low as 9.9 kPa and wind speeds exceeding 20 m/s as measured at the NOAA Prudhoe Bay, AK station. Conversely, the first polar high cyclones that we considered occurred in early November 2019 (shown in Figure 3b). Event 2, occurred on 10 November 2019 a cyclone with pressures that exceeded 10.35 kPa traveled southeast from the northern edge of the East Siberian Sea. Thus, reaching the Chukchi Sea on November 10th with pressure surpassing 10.6 kPa and with measured winds reaching speeds higher than 15 m/s as measured at the NOAA Prudhoe Bay station. It then moved west on November 14th and later declined significantly before completely dissipating on 15 November 2019. The second polar high cyclone, Event 4, that we considered in this study, occurred in the beginning of December 2019 (shown in Figure 4d). This cyclone started to form in the Arctic Ocean on 8 December 2019 where it continued southeast to the Canadian archipelago on 9 December 2019 with pressures higher than 10.45 kPa and wind velocity reaching speeds as high as 21 m/s at the NOAA Prudhoe

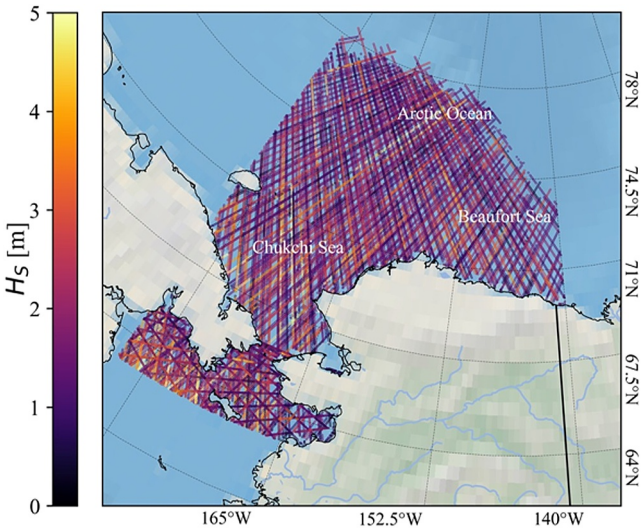

Figure 4. European Space Agency (ESA) Climate Change Initiative (CCI) Sea State Daily Multisensor L3 swath paths from October to December 2019. The data coverage for the Chukchi Sea, Beaufort Sea, and partially of the Arctic Ocean.

Bay station. This cyclone became stagnant in the Beaufort Sea near Banks Island, Canada until 10 December 2019. It then started to dissipate while it began moving southeast to Canada on 12 December 2019.

2.4. Model Evaluation

Observations of the current and historic sea state are a topic of academic interest, notably in the arctic domain. Advancements in remote sensing are allowing a better understanding of the sea state climate in areas where it is difficult to deploy sensors (Squire, 2020; Wadhams et al., 2018). Remote sensing products of the sea states, especially the wave heights, provide validated data that is consistently tested and used for validation of numerical models (Ardhuin et al., 2019; Stopa et al., 2018). In this study, we used wave measurements from the European Space Agency (ESA) Climate Change Initiative (CCI) Sea State Daily Multisensor L3 (Dodet et al., 2020). The ESA CCI product provides reliable, well documented wave height observations in open-water regions, making it a suitable data source to evaluate the predicted wave heights in the Arctic. To ensure the quality of the data and minimize sea ice contamination, the measurements were filtered to exclude areas with sea ice fraction greater than 10%. This filtering step is automatically applied to the measurements (as described by Dodet et al. (2020)) to retain observations that are representative of open-water conditions and reducing the possible bias sea ice can have on the measurements. Finally, the filtered satellite data was used to assess the performance of the different sea ice products within our model framework for simulating wave heights. The measured data was compared to the nearest model node within to ensure alignment with model predictions. The domain of these observations can be seen in Figure 4, where it shows the spatial coverage obtained from the satellite for the study temporal period (October–December 2019).

The significant wave height (Hs) generated by each model setup, encompassing all meteorological events, and parameterized with each of the four sea ice products described above, were assessed with respect to the observations by finding the nearest numerical mesh node to the observation coordinates. A two dimensional Taylor diagram (Taylor, 2001) was used to summarize the statistical performance of the sea ice products relative to the observations during each event discussed earlier. The performance of each product (f) to the observations (r) are evaluated through the center patterned root mean square difference (E'), correlation coefficient (R), and the standard deviation of the model field (σ_f) and reference field (σ_r), which is defined as follows:

$$E' = \left(\frac{1}{N} \sum_{n=1}^{N} \left[(f_n - f) - (r_n - r) \right]^2 \right)^{\frac{1}{2}} \tag{3}$$

$$R = \frac{\frac{1}{N} \sum_{n=1}^{N} (f_n - f) - (r_n - r)}{\sigma_f \sigma_r} \tag{4}$$

$$\sigma_f^2 = \frac{1}{N} \sum_{n=1}^{N} (f_n - f)^2 \tag{5}$$

$$\sigma_r^2 = \frac{1}{N} \sum_{n=1}^{N} (r_n - r)^2 \tag{6}$$

The Taylor diagram is interpreted by the distance to the observations along the x-axis (RMSE), the correlation by the azimuthal position, and the standard deviation is proportional to the radial distance to the observations. This diagram determines the statistical accuracy of the individual products to the observations for the four events.

10.1029/2024EA003803

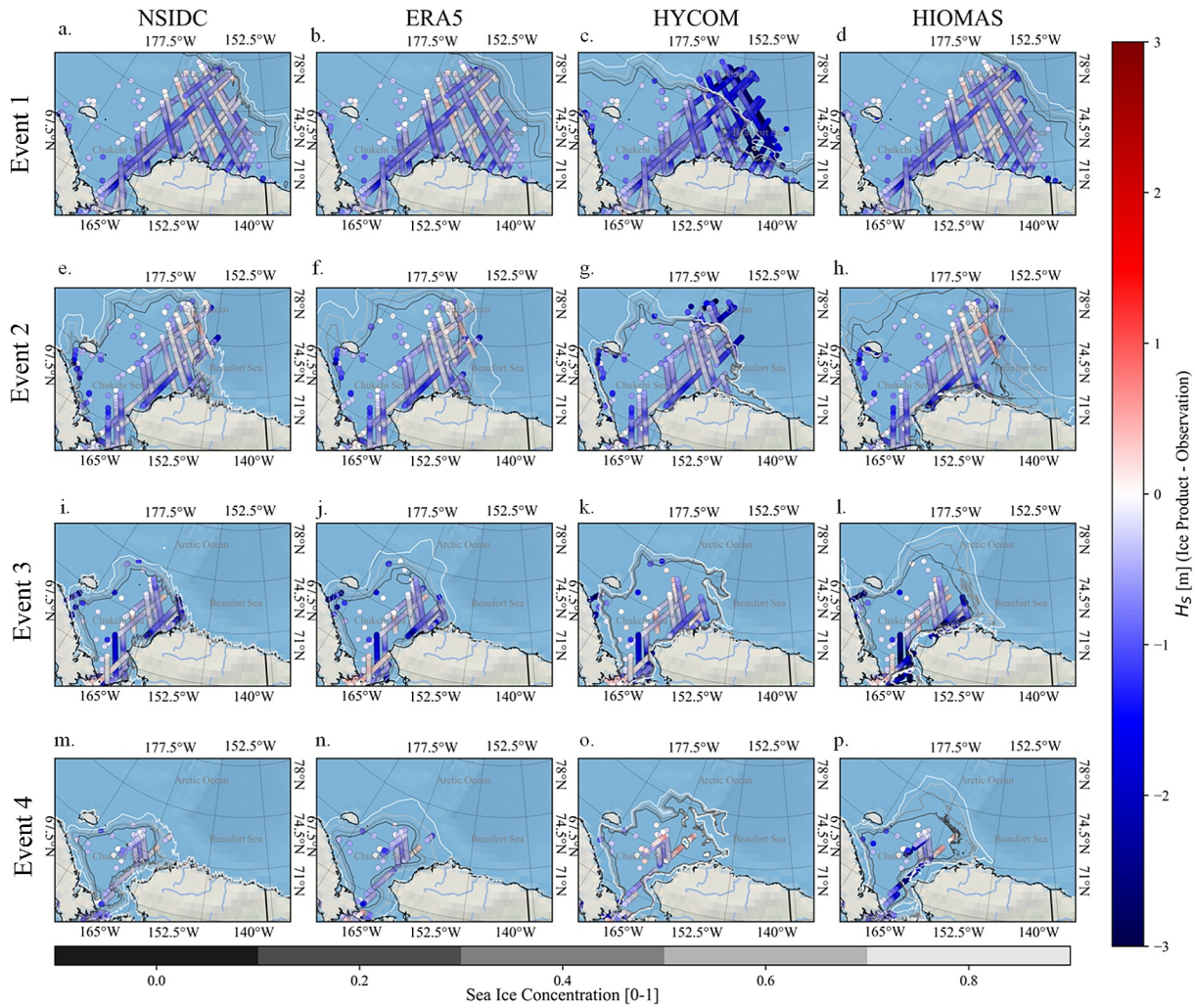

Figure 5. The difference of the extracted max. wave height 2.5 days before and after the peak of each event to the L3 swath ocean climate Hs data. The contour lines represent the sea ice concentration of the corresponding sea ice product during the same event.

3. Results

3.1. Wave Model Validation

Comparing the observations and the modeling results during the selected events from Fall 2019, our analysis reveals variations in simulated Hs. Figures 5 and 6 show a comparison between the modeled wave heights and the satellite observations during a 5-day range of the peak Hs of each event near Alaska, estimated two and a half days before and after the peak wave height. During the almost ice-free conditions in Event 1 (Figures 2a–2d), the wave model was able to reproduce the observed wave heights with an average 0.5 m bias (shown in Figure S2a in Supporting Information S1). In Figures 5a–5d shows differences between the wave heights affected by each sea ice product due to varying sea ice extents in the Arctic Ocean during October, but in the Beaufort and Chukchi Seas the waves are accurately represented in the model to the observations. HYCOM overestimates the sea ice extent in October (can be seen in Figures 2a–2d and Figures S1a–S1d in Supporting Information S1) causing the waves to be underestimated in the MIZ, and larger differences in the Beaufort Sea (Figure 5c). As the sea ice starts to encroach into the Beaufort and Chukchi Seas we start to see disparities between the products.

Event 2 (Figures 6e–6h) generated the lowest Hs at 5.5 m compared to Event 3, where we see the mean biases of each sea ice product ranging within 0.6 m in comparison to the observations (shown in Figure S2b in Supporting Information S1). The Chukchi Sea and the MIZ show the most disparities to the observations (Figures 5e–5h). In the MIZ the products are underestimating the Hs while in the open water area in the Chukchi the Hs is consistent

10.1029/2024EA003803

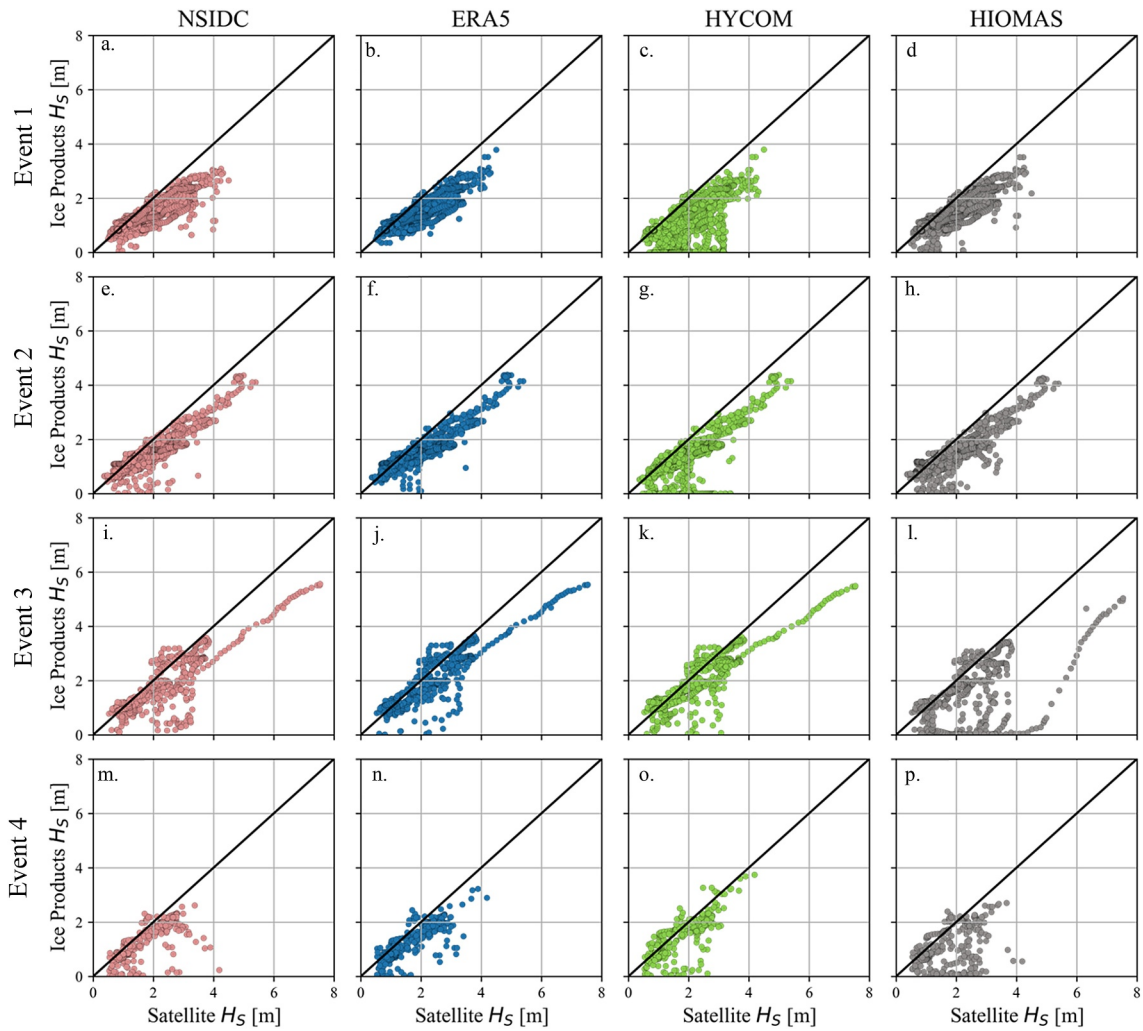

Figure 6. The extracted max. wave height 2.5 days before and after the peak of each event that was cross referenced to the L3 swath ocean climate Hs data based on the time and location.

with the observations. Of all meteorological events shown, Event 3 (Figure 3c) generated the largest Hs with nearly 7.5 m near the Northwest coast of Alaska in the Chukchi Sea, according to satellite observations. Our model predicted significant wave heights, although it underrepresents the Hs that was captured by the satellites in some areas by an average bias of 0.4 m (Figure S2c in Supporting Information S1), simulating a maximum Hs of 6.2 m during the storm peak (Figures 5i–5l) regardless of differences in ice coverage from each model. Each product had slightly overestimated the Hs in the Chukchi Sea (Figures 6i–6l), while the products underestimated the Hs along coastlines. HIOMAS (Figures 5l and 6l) shows considerably more underestimation in the Hs on the Northwest coastline in Alaska. The final event, Event 4 (Figure 3d), where a polar high cyclone event generated waves near the north-west Alaskan Coast. The waves generated for this event (shown in Figures 6m–6p) estimated to be 2.7 m while the simulated Hs had an average bias of 0.55 m (Figure S2d in Supporting Information S1). HYCOM (Figures 5o and 6o) has the highest correlation to the observations near the MIZ that is in the Chukchi Sea. During the open water period the modeled waves provided reasonably accurate to the observations (Figures 5a–5d and 6a–6d). However, as the sea ice encroached during Events 3 and 4 the accuracy of all the simulated waves slightly decreased. Each wave model, with the sea ice products shown in Table 1, proved to have a high correlation and low error relative to the satellite observations during the events where sea ice invaded the domain.

Table 3
Taylor Statistics for the Four Events

		NSIDC	ERA5	HYCOM	HIOMAS	Observations
Event 1	Correlation	0.86	0.89	0.53	0.86	1.00
	SDEV	0.49	0.50	0.79	0.53	0.72
	RMSE	0.39	0.36	0.73	0.38	0.00
Event 2	Correlation	0.91	0.93	0.79	0.89	1.00
	SDEV	0.68	0.66	0.80	0.67	0.87
	RMSE	0.37	0.36	0.54	0.41	0.00
Event 3	Correlation	0.85	0.90	0.89	0.54	1.00
	SDEV	0.95	0.94	0.93	1.04	1.15
	RMSE	0.61	0.52	0.54	1.05	0.00
Event 4	Correlation	0.74	0.83	0.79	0.40	1.00
	SDEV	0.66	0.65	0.76	0.75	0.78
	RMSE	0.53	0.43	0.49	0.84	0.00

3.2. Skill Assessment of the Sea Ice Products

We also compared the model results based on each of the sea ice products to the satellite observations using a statistical skill assessment, shown in Table 3. Where we then applied this diagram over all the observation measurements during the same temporal period for each event.

Table 3 shows that during Event 1, three of the sea ice products emerging Hs have a correlation that ranges between 0.86 and 0.90 with an RMSE of less than 0.39 m. Additionally, these sea ice products' Hs show a standard deviation difference less than 0.23 m compared to the observation. However, HYCOM has a lower Hs correlation nearly 0.53 with an RMSE of 0.73 m, and a standard deviation higher than the observation, with a difference of 0.07 m.

The Event 2, sea ice started encroaching into the model domain inhibiting the wave generation from the polar high cyclone coming from the Arctic Ocean. In Table 3, all the sea ice products' resulting Hs have a correlation [0.79–0.93] and a RMSE that is greater than 0.3 m. Three of the sea ice products (NSIDC, ERA5, HIOMAS) Hs maintains a maximum difference in standard deviation of 0.21 m lower than the observation, while HYCOM's standard deviation is 0.07 m below the observation. Looking at the highest Hs event in this study, Event 3, the sea ice is now extended to the edge of the Chukchi Sea. Here we see in Table 3 that the correlation to the observations [0.85–0.90], and the RMSE has increased to 0.61 m and a similar standard deviation to the last event, 0.22 m. However, HIOMAS has a correlation of 0.56, and a RMSE 1.05 m. During the last event in this study, Event 4, the sea ice is now within the Chukchi Sea and has completely covered the Beaufort Sea. In Table 3, NSIDC, ERA5, and HYCOM Hs have the highest correlation greater than 0.74 and RMSE range [0.43–0.53 m]. The standard deviation to the observations of these three sea ice products Hs have increased in accuracy between [0.65–0.76]. HIOMAS has an Hs correlation of 0.40 with an RMSE 0.84 m. However, the standard deviation of the Hs from HIOMAS to the observations stayed within the same deviation range as the other three sea ice products.

3.3. Influence of Sea Ice Extent on Simulating Waves

The previous results show differences between the sea ice products compared to observations, to further explain these differences we investigate the products' spatial influence on the wave model. Figure 7 depicts the maximum Hs of the 5 day range of the peak of the storm that was described in the validation section. This figure also shows the sea ice concentration at the peak of the corresponding event. To demonstrate how sea ice concentration and extents vary depending on the products during the same temporal period.

The storm that occurred in Event 1 (Figures 7a–7d) resulted in Hs reaching up to 2.5 m in the Beaufort Sea (10 km from Alaskan coastline). During this event, three products showed similar sea ice coverage, with partial cover in the Arctic Ocean and the Beaufort Sea (Figures 7a, 7b, and 7d; Figures S1a, S1b, and S1d in Supporting Information S1). However, HYCOM (Figure 7c) presents an anomalous estimation of sea ice in comparison to the other products (NSIDC, ERA5, and HIOMAS), which completely covers the Arctic Ocean and a portion of the Beaufort Sea, thus constraining Hs on the coasts due to reduction in the fetch length. On the other hand, Event 2 (Figures 7e–7h), was a polar high cyclone that propagated waves from the Arctic Ocean toward the coast of Alaska. During that time, the sea ice had covered the majority of the central Arctic Ocean and the Beaufort Sea. Here, NSIDC, ERA5, and HIOMAS (Figures 7e, 7f, and 7h) produced similar sea ice extents with slight differences in the spatial variability of the concentrations, although HIOMAS has the sea ice concentration spatially spread from 152.5° to 136°W. At this time HYCOM (Figure 7g) continues to show an overestimation in sea ice extent compared to the other products, but even though there is an overestimation in the sea ice extent, it shows no substantial sea ice along the coast of Alaska until after 145°W. The Hs generated by the polar high cyclone, Event 3, reached 5m in the Chukchi Sea, while the Hs near the Alaskan coast was limited due to the presence of sea ice, reaching an estimated 1.5 m Hs. In the previous section, it was mentioned that Event 3 generated the highest Hs, notably in the Chukchi Sea (Figures 7i–7l). During this event, HIOMAS (Figure 7l) is fully attenuating the Hs along the coast due to the presence of high sea ice concentration, while the other products do show sea ice near the coast, the concentration is lower than HIOMAS. Differences in the generated Hs are observed near the MIZ due to the variation in sea ice concentration with ERA5 and HIOMAS (Figures 7j and 7l) having a larger spatial

10.1029/2024EA003803

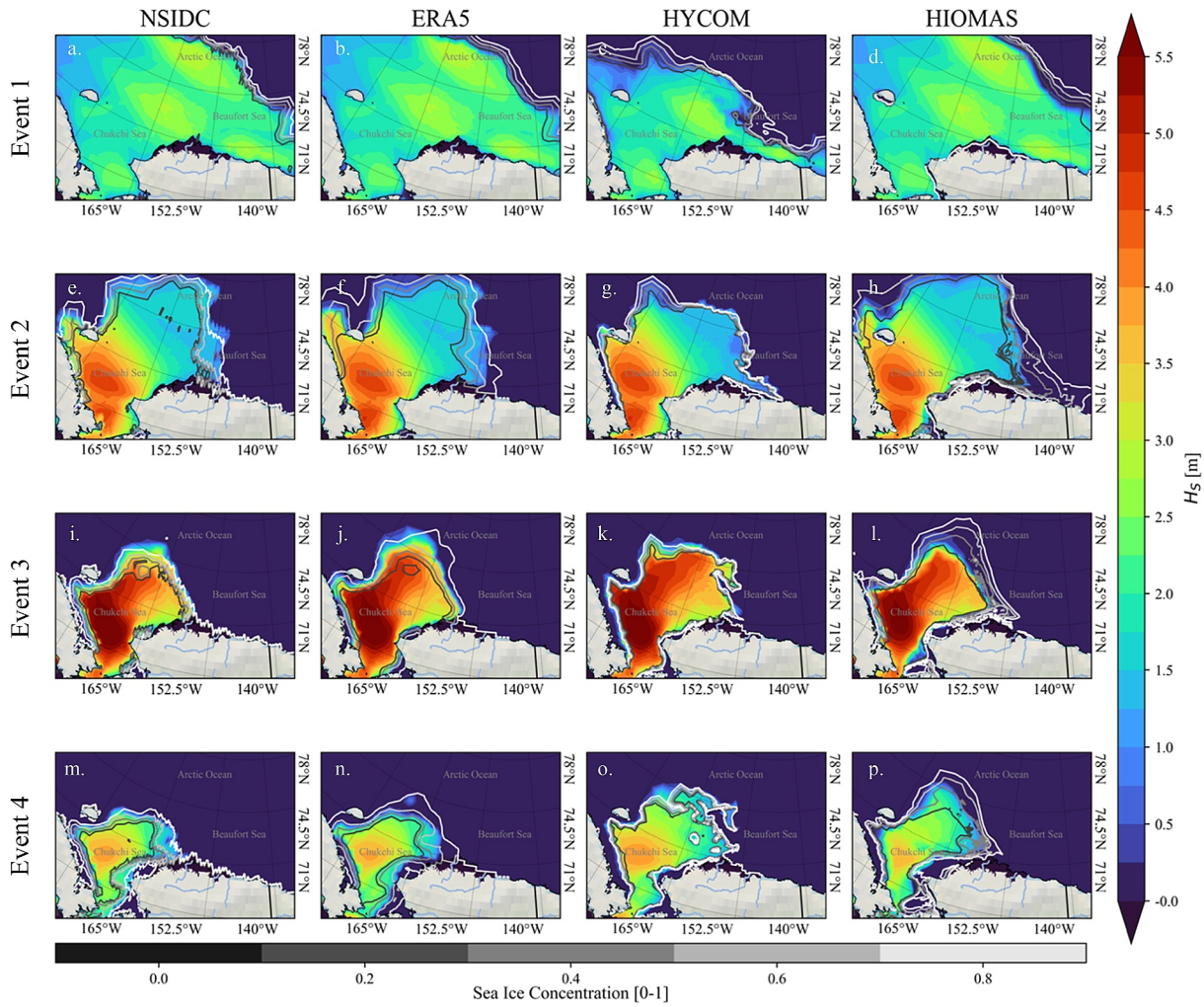

Figure 7. The extracted max. wave height 2.5 days before and after the peak of each event. The contour lines represent the corresponding the sea ice concentration from the sea ice products during the same temporal period.

distribution in the concentration. The last event in this study, Event 4 (Figures 7m–7p), shows the sea ice extent at the Chukchi Sea while the largest Hs (4m) was generated on the western side of the Chukchi Sea. HYCOM (Figure 7o) shows the largest spatial variability in sea ice extent, while NSIDC (Figure 6m) has the greatest sea ice extent. ERA5 and HIOMAS (Figures 7n and 7p) continued to have a large spread in the sea ice concentration resulting in a more gradual wave generation than the other products.

3.4. Ensemble Model Hs Comparison

We compared the differences in the resulting Hs for each of the sea ice products, focusing on where individual products diverge. Figure 8 shows the ensemble difference for maximum Hs near the peak of the event, spanning a 5-day period where the maximum Hs for each node was extracted. In this context, when the Hs appears blue, it indicates an underestimation in the Hs influenced by greater sea ice coverage; conversely, red represents an Hs overestimation influenced by a reduced amount of sea ice coverage.

During the first event in this study (Figures 8a–8d), there was limited sea ice resulting in minimal variation in fetch driven waves between the products. However, HYCOM (Figure 8c) displayed a notable divergence due to the more extensive MIZ in the Beaufort and Chukchi Seas. This can also be seen in Figure S1c in Supporting Information S1, showing that the sea ice concentration is different to the ensemble average. However, even though HYCOM overestimates the sea ice in the open water areas, the area near the Alaskan coast shows little to no differences in Hs. As the sea ice starts to encroach into our domain for Event 2 (Figures 8e–8h), the products

10.1029/2024EA003803

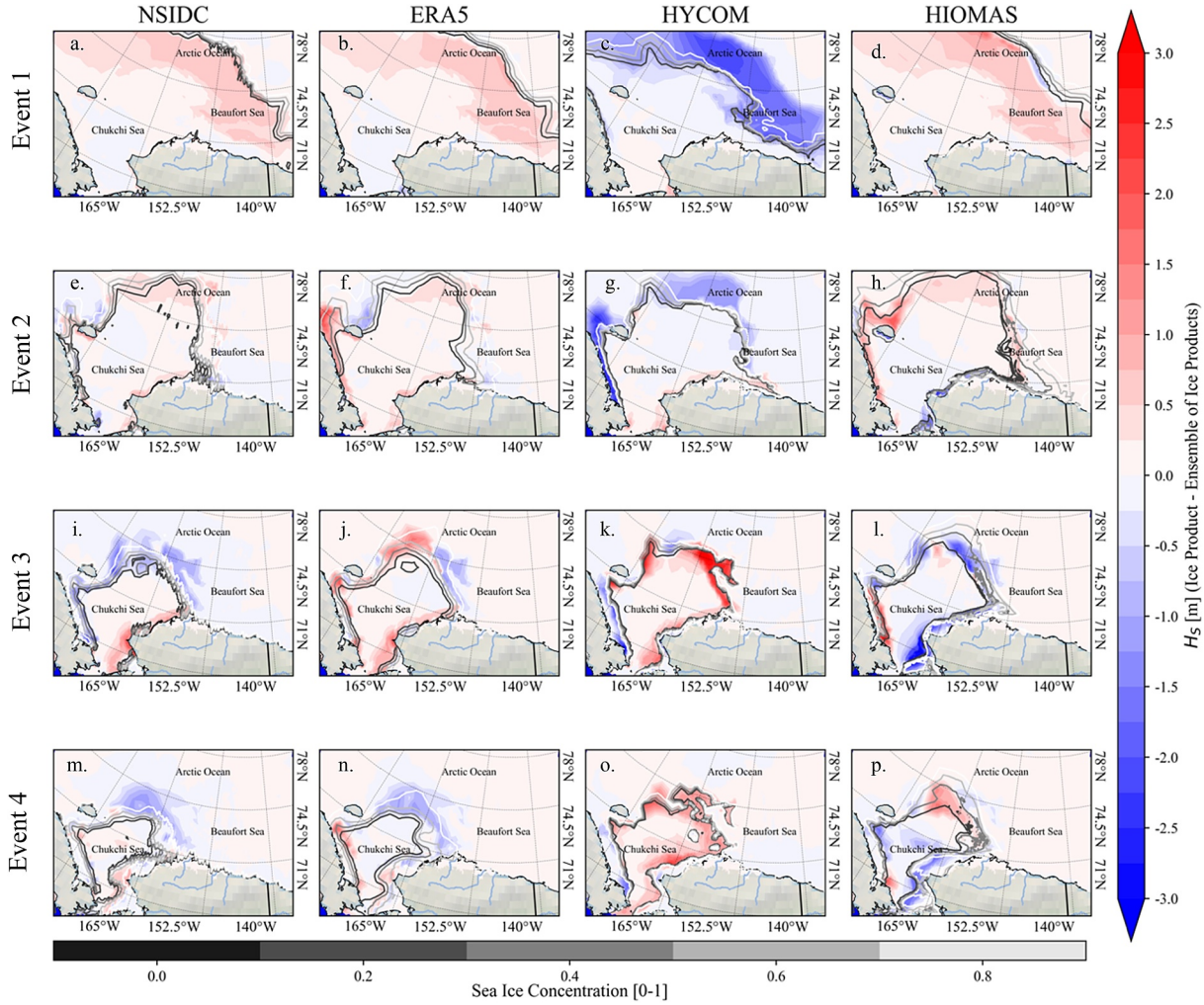

Figure 8. The difference to the ensemble average wave height of all the products to the extracted max. wave height 2.5 days before and after the peak of each event. The contour lines represent the sea ice concentration of the corresponding sea ice product during the same temporal period.

show in the MIZ there are differences in the Hs, with HYCOM (Figure 8g) having the majority of the differences due to having a smaller distribution in sea ice concentration than the other sea ice products. HYCOM and HIOMAS (Figures 8g and 8h) display high concentration of coastal sea ice that is completely attenuating the Hs along the coastline, while the ERA5 and NSIDC (Figures 8e and 8f) do not include overland ice (or landfast ice) they do show that the sea ice extent has covered over half of the Alaskan coast. The largest event in this study, Event 3 (Figures 8i–8l), shows the majority of the differences around the outer edge of the Chukchi Sea, which transitions to both the East Siberian Sea and the Beaufort Sea. The MIZ in this temporal period has encroached to the Chukchi Sea and here is where the products differ from each other between the sea ice concentration to the varying extent of the MIZ. Notable differences can be seen in the Beaufort Sea, north of the Alaskan coast, and along the coastline of Alaska with Hs differences reaching higher than 2m. ERA5 sea ice results in lower Hs differences in the MIZ, whereas HYCOM sea ice is resulting in larger Hs differences in the MIZ due to open water area being larger than the other three sea ice products. Moving to the coastline in Alaska, HIOMAS sea ice has the Hs going to zero causing underestimation in the Hs compared to the ensemble, which can be seen with the other products simulating Hs in these areas (earlier HIOMAS provided the lowest correlation to observations during the Event 3, Table 3). In contrast to Event 3, Event 2 show that the sea ice products had the least number of differences from the ensemble. The last event, Event 4 (Figures 8m–8p), the sea ice products show the MIZ has now completely covered the Arctic Ocean, the Beaufort Sea, and the coast of Alaska. Furthermore, each product shows varying spatial differences in the MIZ that has encroached unto the Chukchi Sea. Notably, NSIDC (Figure 8m)

10.1029/2024EA003803

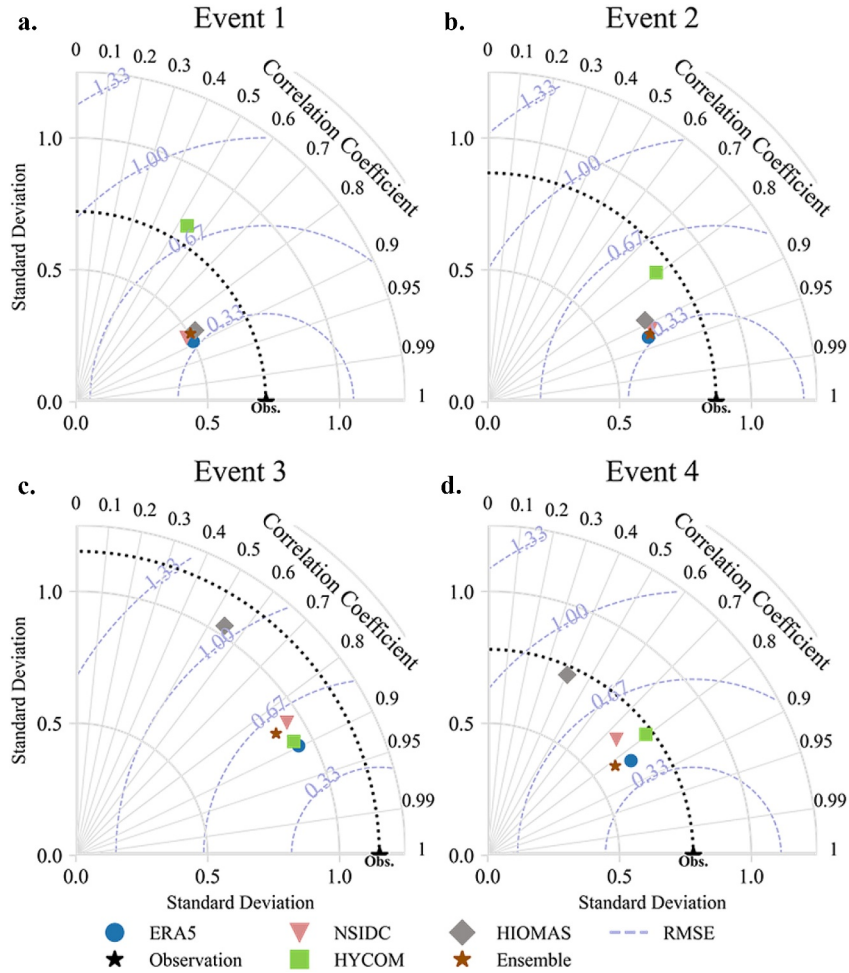

Figure 9. Taylor Diagram that describe the skill of each product and the ensemble of the sea ice products in comparison to the L3 swath ocean climate data. (a) Event 1: wind event. (b) Event 2: polar high cyclone. (c) Event 3: polar low cyclone. (d) Event 4: polar high cyclone.

and ERA5 (Figure 8n) show broad sea ice coverage, while HYCOM (Figure 8o) underestimates the extent of the MIZ, leading to larger Hs predictions in the Chukchi Sea, exceeding 3 m in some areas. HIOMAS (Figure 8p) shows a more spatial distribution in the sea ice concentration similar to ERA5, but it underestimates the Hs along the coastline.

The statistical skill of the sea ice products, as detailed in Table 3, was compared to observational data and visualized in a Taylor Diagram in Figure 9. This figure shows the statistical skill of the Hs resulting from the individual sea ice products and the ensemble for the four events analyzed in this study. For the near ice-free Event 1 (Figure 9a), the ensemble, NSIDC, ERA5, and HIOMAS products all demonstrated a Hs correlation above 0.8 with the observations. In Figure S2a in Supporting Information S1, the bias distribution shows the resulting Hs from HYCOM having a larger spread of bias points being underestimated affecting the distribution of the ensemble bias. During Event 2 (Figure 9b), as sea ice began to cover the Beaufort Sea, the Hs from the sea ice products increased in accuracy compared to the observations, though the ensemble had a slightly lower correlation than ERA5. In Event 3 (Figure 9c), the correlation of Hs from the sea ice products with observations decreased, although ERA5, HYCOM, and the ensemble maintained a correlation greater than 0.87. The distribution of the bias (Figure S2c in Supporting Information S1) shows HIOMAS having a considerable spread in the bias offsetting the distribution of the ensemble. For Event 4 (Figure 9d), ERA5 exhibited the highest Hs correlation with the observations, with the ensemble following closely behind. Similar to Event 3, the distribution in the sea ice concentration in HIOMAS has increased affecting the ensemble in comparison to the observations

(Figure S2d in Supporting Information S1). Overall, the ensemble demonstrated high accuracy across all events, but ERA5 resulted in the highest Hs accuracy for all four events when compared to the observations.

4. Discussions and Conclusions

In this study we used a varying resolution ADCIRC + SWAN model that was simulated with ERA5 winds and pressure fields for October–December 2019, where we validated Hs against satellite Hs observations. Furthermore, we incorporated sea ice from four different products using the IC4M2 method described in Rogers (2019) to account for the growth and dissipation of waves in sea ice conditions. We evaluated how spatially and temporally varying sea ice products influence wave propagation in the Arctic. The model performance of the wave regime in the Arctic for the different sea ice products were assessed using Taylor diagrams, statistical skill comparison, and event peak comparison. Moreover, an ensemble analysis was performed to delineate regions where individual products within the ensemble diverge from the collective average. Using these methods, we determined:

1. The wave model was validated against observed Hs from Sea State Daily Multisensor L3 satellite data with an estimated average accuracy of 80% for all events in this study (shown in Figures 6 and 9).
2. ERA5 showed consistent high skill in the resulting Hs during all events in this study, maintaining over 83% correlation, when we compared the modeled Hs to the satellite observations (shown in Figures 6 and 9).
3. HYCOM was consistently the second highest Hs of the four sea ice products in correlation to the observations for Events 3 and 4 where sea ice coverage was greatest.
4. ERA5 and HIOMAS produce a spatially dispersed sea ice concentration versus the other products resulting in the sea ice having a more incremental impact.
5. The sea ice products yield differences in Hs in the MIZ and near the Alaskan coast. HIOMAS underestimates the Hs, while HYCOM overestimates the Hs in the last two events.
6. ERA5 and NSIDC provide similar sea ice representations (Figures 8i, 8j, 8m, and 8n) to the sea ice product ensemble resulting in comparable Hs during the last two Events in this study.
7. The ensemble of the sea ice products produced consistently high Hs correlation to the observations, albeit lower than ERA5.

The wave model was able to accurately simulate the Hs in the study domain for Event 1 when sea ice was almost nonexistent in the study domain. Except for HYCOM, with overestimation in sea ice extent, the other sea ice products estimated similar sea ice extents allowing the models' Hs to correlate with the satellite observations (Figure 9a). As the sea ice encroaches onto the study domain the correlation to the observation increases in Event 2, but slightly decreases for the last two events when the sea ice has significant dynamic changes (Figures 8b and 8c). The four sea ice products yield different sea ice extents for Events 2 and 3 which is evident in Figure 8 where the MIZ has the largest impact at this time. One potential source for the disparity between the model and the observations when sea ice is present is the wave model using the IC4M2 empirical wave attenuation. Yang et al. (2024) discuss its high accuracy for local scale studies where specific sea ice is present. However, on larger domains, the wave attenuation is spatially variable depending on sea ice properties. Squire (2020) elaborates on the empirical parameterizations and the need for improvements to enhance the accuracy of the wave dissipation processes in sea ice conditions.

Our results showed how the spatial and temporal differences of the sea ice extents in the different products impacted the wave generation and the dissipation of the wave energy. In Figure 8, the sea ice extent along with the difference in Hs highlights unique characteristics of the sea ice products, especially along the MIZ and the coast of Alaska. The spatially varying sea ice is an important feature when modeling waves in the arctic domain, but the dissipation methods available are meant for specific sea ice conditions in a given spatial domain. The high-resolution sea ice products did not show any notable difference to the coarser sea ice products at this domain, but these high resolution products can be crucial for smaller-scale studies. For example, Hošeková et al. (2021) and Nederhoff et al. (2022) show that sea ice resolution is a key feature when modeling waves nearshore. These studies used ERA5 sea ice where Nederhoff et al. (2022) discuss the lack of landfast ice and the underestimation of sea ice during the various seasons. As for Hošeková et al. (2021), they interpolated a Landfast ice mask to ERA5 sea ice from HYCOM to improve the bias of ERA5's underestimation of sea ice in coastal areas. Landfast ice is a key feature in coastal studies that include overland components. With the method Hošeková et al. (2021) instituted in their study, it reduced the bias of the wave response nearshore. When looking at smaller scale studies, HIOMAS and/or HYCOM will have sea ice extents and concentrations with a better representation, including the

sea ice along the coast versus a coarser resolution product that doesn't include such features like ERA5 and NSIDC.

Sea Ice is a crucial component when modeling hydrodynamics and waves in the arctic, and with increased precision in the representation to the observed sea ice conditions, the accuracy of estimating the potential hazards in the Arctic will increase. The sea ice products can be seen by the unique characteristics with the comparison to the ensemble of the sea ice products (Figure 8). This highlights the differences between the sea ice products and the unique characteristics that will benefit further studies in either the MIZ or the coastal zones in the Arctic. Additionally, we showed that the ensemble of the sea ice products did not show any notable increase in accuracy for the four events in this study. In Figure S2 in Supporting Information S1, the outlying products for the each event affects the accuracy of the ensemble and different ensemble combinations may provide higher accuracy. However, due to limits on computational resources and the results of the high accuracy of ERA5 this was not pursued. During the transitioning fall to winter season, where the sea ice is growing from the Arctic Ocean to the Chukchi Sea, incorporating a sea ice product will increase the accuracy of the wave response in the Arctic regime. Advancements in both sea ice parameterizations and wave induced sea ice break up will allow for accurate representations of the wave climate in the arctic.

Data Availability Statement

Data for the sea ice concentration is available from the European Centre for Medium-Range Weather forecasts (C3S, 2018), the National Snow and Ice Data Center (DiGirolamo et al., 2022), HYCOM-CICE (Barton et al., 2021), and HIOMAS (data available through contacting uaa.adac@alaska.edu). The numerical model ADCIRC-SWAN that is used to simulate the wave hazards influenced by the sea ice products is available at https://github.com/adcirc/adcirc (Westerink et al., 1992). The wave simulation data used in this analysis is available at the Designsafe data repository (Miesse, 2024).

Acknowledgments
The authors wish to thank the Texas Advanced Computing Center (TACC) of The University of Texas at Austin for providing the high-performance computing resources necessary. In this work, we utilized the Extreme Science and Engineering Discovery Environment (XSEDE) STAMPEDE3 resources through allocation id TG-BCS130009, which is supported by National Science Foundation (Grant 1927785).

References

Ardhuin, F., Stopa, J. E., Chapron, B., Collard, F., Husson, R., Jensen, R. E., et al. (2019). Observing sea states. *Frontiers in Marine Science*, *6*, 124. https://doi.org/10.3389/fmars.2019.00124

Barton, N., Metzger, E. J., Reynolds, C. A., Ruston, B., Rowley, C., Smedstad, O. M., et al. (2021). The Navy's Earth System Prediction Capability: A new global coupled atmosphere-ocean-sea ice prediction system designed for daily to subseasonal forecasting. *Earth and Space Science*, *8*(4), e2020EA001199. https://doi.org/10.1029/2020EA001199

Blanton, B., Stillwell, L., Roberts, H., Atkinson, J., Zou, S., Forte, M., et al. (2011). Coastal Storm Surge Analysis: Computational System Coastal and Hydraulics Laboratory Coastal Storm Surge Analysis: Computational System (Vol. *1*).

Booij, N., Ris, R. C., & Holthuijsen, L. H. (1999). A third-generation wave model for coastal regions. *Journal of Geophysical Research*, *104*(C4), 7649–7666. https://doi.org/10.1029/98jc02622

Branch, R., García-Medina, G., Yang, Z., Wang, T., Ticona Rollano, F., & Hosekova, L. (2021). Modeling sea ice effects for wave energy resource assessments. *Energies*, *14*(12), 1–15. https://doi.org/10.3390/en14123482

Buzard, R. M., Maio, C. V., Erikson, L. H., Overbeck, J. R., Kinsman, N. E. M., & Jones, B. M. (2024). Current and projected flood exposure for Alaska coastal communities. *Scientific Reports*, *14*(1), 7765. https://doi.org/10.1038/s41598-024-58270-w

C3S. (2018). ERA5 hourly data on single levels from 1940 to present [Dataset]. *Copernicus Climate Change Service (C3S) Climate Data Store (CDS)*. https://doi.org/10.24381/CDS.ADBB2D47

Cassalho, F., Miesse, T. W., Khalid, A., de Lima, A. D. S., Ferreira, C. M., Henke, M., & Ravens, T. M. (2022). Intercomparing atmospheric reanalysis products for hydrodynamic and wave modeling of extreme events during the open-water Arctic season. *Arctic, Antarctic, and Alpine Research*, *54*(1), 125–146. https://doi.org/10.1080/15230430.2022.2059957

Cavalieri, D., Parkinson, C., Gloersen, P., & Zwally, H. J. (1996). Sea Ice Concentrations from Nimbus-7 SMMR and DMSP SSM/I-SSMIS Passive Microwave Data, Version 1 [Dataset]. *NASA National Snow and Ice Data Center Distributed Active Archive Center*. https://doi.org/10.5067/8GQ8LZQVL0VL

Collard, F., Marié, L., Nouguier, F., Kleinherenbrink, M., Ehlers, F., & Ardhuin, F. (2022). Wind-wave attenuation in Arctic sea ice: A discussion of remote sensing capabilities. *Journal of Geophysical Research: Oceans*, *127*(7), e2022JC018654. https://doi.org/10.1029/2022JC018654

Collins, C., & Rogers, W. E. (2017). *A source term for wave attenuation by sea ice in WAVEWATCH III®: IC4*. Naval Research Laboratory.

Comiso, J. C., & Nishio, F. (2008). Trends in the sea ice cover using enhanced and compatible AMSR-E, SSM/I, and SMMR data. *Journal of Geophysical Research*, *113*(C2), 2007JC004257. https://doi.org/10.1029/2007JC004257

Danielson, J. J., Poppenga, S. K., Brock, J. C., Evans, G. A., Tyler, D. J., Gesch, D. B., et al. (2016). Topobathymetric elevation model development using a new methodology: Coastal national elevation database. *Journal of Coastal Research*, *76*(sp1), 75–89. https://doi.org/10.2112/SI76-008

Dewitz, J. (2021). National Land Cover Database (NLCD) 2019 Products [Dataset]. *U.S. Geological Survey*. https://doi.org/10.5066/P9KZCM54

Dietrich, J. C., Tanaka, S., Westerink, J. J., Dawson, C. N., Luettich, R. A., Zijlema, M., et al. (2012). Performance of the unstructured-mesh, SWAN+ADCIRC model in computing hurricane waves and surge. *Journal of Scientific Computing*, *52*(2), 468–497. https://doi.org/10.1007/s10915-011-9555-6

DiGirolamo, N. E., Parkinson, C. L., Cavalieri, D. J., Gloersen, P., & Zwally, H. J. (2022). Sea Ice Concentrations from Nimbus-7 SMMR and DMSP SSM/I-SSMIS Passive Microwave Data [Dataset]. *NASA National Snow and Ice Data Center Distributed Active Archive Center*. https://doi.org/10.5067/MPYG15WAA4WX

Dodet, G., Piolle, J.-F., Quilfen, Y., Abdalla, S., Accensi, M., Ardhuin, F., et al. (2020). The Sea State CCI dataset v1: Towards a sea state climate data record based on satellite observations. *Earth System Science Data*, *12*(3), 1929–1951. https://doi.org/10.5194/essd-12-1929-2020

Donlon, C. J., Martin, M., Stark, J., Roberts-Jones, J., Fiedler, E., & Wimmer, W. (2012). The Operational Sea Surface Temperature and Sea Ice Analysis (OSTIA) system. *Remote Sensing of Environment*, *116*, 140–158. https://doi.org/10.1016/j.rse.2010.10.017

Eastwood, S., Lavergne, T., & Tonboe, R. (2014). Algorithm theoretical basis document for the OSI SAF global reprocessed sea ice concentration product, *He EUMETSAT Network of Satellite Application Facilities*.

Ferreira, C. M., Irish, J. L., & Olivera, F. (2014). Uncertainty in hurricane surge simulation due to land cover specification. *Journal of Geophysical Research: Oceans*, *119*(3), 1812–1827. https://doi.org/10.1002/2013JC009604

Finocchio, P. M., Doyle, J. D., Stern, D. P., & Fearon, M. G. (2020). Short-term impacts of Arctic summer cyclones on sea ice extent in the marginal ice zone. *Geophysical Research Letters*, *47*(13), e2020GL088338. https://doi.org/10.1029/2020GL088338

Forbes, D. L., & Taylor, R. B. (1994). Ice in the shore zone and the geomorphology of cold coasts. *Progress in Physical Geography: Earth and Environment*, *18*(1), 59–89. https://doi.org/10.1177/030913339401800104

Gorrell, L., Raubenheimer, B., Elgar, S., & Guza, R. T. (2011). SWAN predictions of waves observed in shallow water onshore of complex bathymetry. *Coastal Engineering*, *58*(6), 510–516. https://doi.org/10.1016/j.coastaleng.2011.01.013

Hartmuth, K., Papritz, L., Boettcher, M., & Wernli, H. (2023). Arctic seasonal variability and extremes, and the role of weather systems in a changing climate. *Geophysical Research Letters*, *50*(8), e2022GL102349. https://doi.org/10.1029/2022GL102349

Henke, M., Miesse, T., De Lima, A. D. S., Ferreira, C. M., & Ravens, T. M. (2024). Increasing coastal exposure to extreme wave events in the Alaskan Arctic as the open water season expands. *Communications Earth & Environment*, *5*(1), 165. https://doi.org/10.1038/s43247-024-01323-9

Hersbach, H., Bell, B., Berrisford, P., Hirahara, S., Horányi, A., Nicolas, J., et al. (2020). The ERA5 global reanalysis. *Quarterly Journal of the Royal Meteorological Society*, *146*(730), 1999–2049. https://doi.org/10.1002/qj.3803

Hirahara, S., Balmaseda, M. A., Boisseson, E. D., & Hersbach, H. (2016). *26 sea surface temperature and sea ice concentration for ERA5* (ERA Reports Series). European Centre Medium Range Weather Forecasts.

Hošeková, L., Eidam, E., Panteleev, G., Rainville, L., Rogers, W. E., & Thomson, J. (2021). Landfast ice and coastal wave exposure in Northern Alaska. *Geophysical Research Letters*, *48*(22), e2021GL095103. https://doi.org/10.1029/2021GL095103

Hošeková, L., Malila, M. P., Rogers, W. E., Roach, L. A., Eidam, E., Rainville, L., et al. (2020). Attenuation of ocean surface waves in pancake and frazil sea ice along the coast of the Chukchi Sea. *Journal of Geophysical Research: Oceans*, *125*(12), e2020JC016746. https://doi.org/10.1029/2020JC016746

Hume, J. D., & Schalk, M. (1967). Shoreline processes near Barrow, Alaska: A comparison of the normal and the catastrophic. *Arctic*, *20*(2), 86–103. https://doi.org/10.14430/arctic3285

Hunke, E. C., & Lipscomb, W. H. (2010). CICE: The Los Alamos Sea Ice Model Documentation and Software User's Manual Version 4.

Joyce, B. R., Pringle, W. J., Wirasaet, D., Westerink, J. J., Van der Westhuysen, A. J., Grumbine, R., & Feyen, J. (2019). High resolution modeling of western Alaskan tides and storm surge under varying sea ice conditions. *Ocean Modelling*, *141*, 101421. https://doi.org/10.1016/j.ocemod.2019.101421

Kenigson, J. S., & Timmermans, M.-L. (2021). Arctic cyclone activity and the Beaufort High. *Journal of Climate*, *34*(10), 4119–4127. https://doi.org/10.1175/JCLI-D-20-0771.1

Kousal, J., Voermans, J. J., Liu, Q., Heil, P., & Babanin, A. V. (2022). A two-part model for wave-sea ice interaction: Attenuation and break-up. *Journal of Geophysical Research: Oceans*, *127*(5), e2022JC018571. https://doi.org/10.1029/2022JC018571

Kumar, N., Rogers, W. E., Thomson, J., & Collins, C. (2020). Wave-ice interaction for regional applications: SWAN developments and validations [Preprint]. *Oceanography*. https://doi.org/10.1002/essoar.10504399.1

Lindsay, R., & Schweiger, A. (2015). Arctic sea ice thickness loss determined using subsurface, aircraft, and satellite observations. *The Cryosphere*, *9*(1), 269–283. https://doi.org/10.5194/tc-9-269-2015

Liu, J., Xie, H., Guo, Y., Tong, X., & Li, P. (2022). A sea ice concentration estimation methodology utilizing ICESat-2 Photon-Counting Laser Altimeter in the Arctic. *Remote Sensing*, *14*(5), 1130. https://doi.org/10.3390/rs14051130

Metzger, E. J., Hurlburt, H. E., Wallcraft, A. J., Shriver, J. F., Smedstad, L. F., Smedstad, O. M., et al. (2008). Validation Test Report for the Global Ocean Prediction System V3.0 – 1/12° HYCOM/NCODA: Phase I.

Meylan, M. H., Bennetts, L. G., & Kohout, A. L. (2014). In situ measurements and analysis of ocean waves in the Antarctic marginal ice zone. *Geophysical Research Letters*, *41*(14), 5046–5051. https://doi.org/10.1002/2014GL060809

Miesse, T. (2024). *Wave simulation data for the critical role of sea ice products for accurate wind-wave simulations in the Arctic*. Designsafe-CI. https://doi.org/10.17603/DS2-H0FW-2P96

Miesse, T., De Souza De Lima, A., Khalid, A., Cassalho, F., Coleman, D. J., Ferreira, C. M., & Sutton-Grier, A. E. (2023). Numerical modeling of wave attenuation: Implications of representing vegetation found in coastal saltmarshes in the Chesapeake Bay. *Environmental Monitoring and Assessment*, *195*(8), 982. https://doi.org/10.1007/s10661-023-11533-x

Nederhoff, K., Erikson, L., Engelstad, A., Bieniek, P., & Kasper, J. (2022). The effect of changing sea ice on wave climate trends along Alaska's central Beaufort Sea coast. *The Cryosphere*, *16*(5), 1609–1629. https://doi.org/10.5194/tc-16-1609-2022

Overeem, I., Anderson, R. S., Wobus, C. W., Clow, G. D., Urban, F. E., & Matell, N. (2011). Sea ice loss enhances wave action at the Arctic coast. *Geophysical Research Letters*, *38*(17), L17503. https://doi.org/10.1029/2011GL048681

Parker, B., Milbert, D., Hess, K., & Gill, S. (2003). National VDatum -- The implementation of a national vertical datum transformation database. In *Proceeding from the US Hydro'2003 Conference*.

Passeri, D., Hagen, S. C., Smar, D., Alimohammadi, N., Risner, A., & White, R. (2012). Sensitivity of an ADCIRC tide and storm surge model to Manning's *n*. *Estuarine and Coastal Modeling*, *53*(9), 457–475. https://doi.org/10.1061/9780784412411.00027

Posey, P., Metzger, E. J., Wallcraft, A. J., Preller, R. H., Smedstad, O. M., & Phelps, M. W. (2010). Validation of the 1/12 Arctic Cap Nowcast/Forecast System (ACNFS) (Naval Research Lab Report NRL/MR/7320--10-9287).

Posey, P., & Preller, R. H. (1997). The Polar Ice Prediction System (PIPS 2.0) – The Navy's sea ice forecasting system. In *Proceedings of the Seventh International Offshore and Polar Engineering Conference* (pp. 537–543).

Roberts, K. J., Pringle, W. J., & Westerink, J. J. (2019). OceanMesh2D 1.0: MATLAB-based software for two-dimensional unstructured mesh generation in coastal ocean modeling. *Geoscientific Model Development*, *12*(5), 1847–1868. https://doi.org/10.5194/gmd-12-1847-2019

Rogers, W. E. (2019). Implementation of Sea Ice in the Wave Model SWAN.

Serreze, M. C., & Barrett, A. P. (2011). Characteristics of the Beaufort Sea High. *Journal of Climate*, *24*(1), 159–182. https://doi.org/10.1175/2010JCLI3636.1

Serreze, M. C., Walsh, J. E., Chapin Iii, F. S., Osterkamp, T., Dyurgerov, M., Romanovsky, V., et al. (2000). Observational evidence of recent change in the northern high-latitude environment. *Climatic Change*, *46*(1/2), 159–207. https://doi.org/10.1023/A:1005504031923

Short, A. D., & Wiseman, W. J., Jr. (1974). Freezeup processes on Arctic beaches. *Arctic*, *27*(3), 215–224. https://doi.org/10.14430/arctic2875
Squire, V. A. (2018). A fresh look at how ocean waves and sea ice interact. *Philosophical Transactions of the Royal Society A: Mathematical, Physical and Engineering Sciences*, *376*(2129), 20170342. https://doi.org/10.1098/rsta.2017.0342
Squire, V. A. (2020). Ocean wave interactions with sea ice: A reappraisal. *Annual Review of Fluid Mechanics*, *52*(1), 37–60. https://doi.org/10.1146/annurev-fluid-010719-060301
Squire, V. A., & Williams, T. D. (2008). Wave propagation across sea-ice thickness changes. *Ocean Modelling*, *21*(1–2), 1–11. https://doi.org/10.1016/j.ocemod.2007.10.006
Stopa, J. E., Ardhuin, F., Thomson, J., Smith, M. M., Kohout, A., Doble, M., & Wadhams, P. (2018). Wave attenuation through an Arctic marginal ice zone on 12 October 2015: 1. Measurement of wave spectra and ice features from Sentinel 1A. *Journal of Geophysical Research: Oceans*, *123*(5), 3619–3634. https://doi.org/10.1029/2018JC013791
Taylor, K. E. (2001). Summarizing multiple aspects of model performance in a single diagram. *Journal of Geophysical Research*, *106*(D7), 7183–7192. https://doi.org/10.1029/2000JD900719
The SWAN team. (2019). SWAN user manual version 41.31 (p. 143).
Thomson, J., & Rogers, W. E. (2014). Swell and sea in the emerging Arctic Ocean. *Geophysical Research Letters*, *41*(9), 3136–3140. https://doi.org/10.1002/2014GL059983
Urdea, P. (2007). About some geomorphological aspects of the polar beaches.
Valkonen, E., Cassano, J., & Cassano, E. (2021). Arctic cyclones and their interactions with the declining sea ice: A recent climatology. *Journal of Geophysical Research: Atmospheres*, *126*(12), 1–35. https://doi.org/10.1029/2020JD034366
Wadhams, P., Aulicino, G., Parmiggiani, F., Persson, P. O. G., & Holt, B. (2018). Pancake ice thickness mapping in the Beaufort Sea from wave dispersion observed in SAR imagery. *Journal of Geophysical Research: Oceans*, *123*(3), 2213–2237. https://doi.org/10.1002/2017JC013003
Waseda, T., Nose, T., Kodaira, T., Sasmal, K., & Webb, A. (2021). Climatic trends of extreme wave events caused by Arctic Cyclones in the western Arctic Ocean. *Polar Science*, *27*, 100625. https://doi.org/10.1016/j.polar.2020.100625
Waseda, T., Webb, A., Sato, K., Inoue, J., Kohout, A., Penrose, B., & Penrose, S. (2018). Correlated increase of high ocean waves and winds in the ice-free waters of the Arctic Ocean. *Scientific Reports*, *8*(1), 1–9. https://doi.org/10.1038/s41598-018-22500-9
Weatherall, P., Marks, K. M., Jakobsson, M., Schmitt, T., Tani, S., Arndt, J. E., et al. (2015). A new digital bathymetric model of the world's oceans. *Earth and Space Science*, *2*(8), 331–345. https://doi.org/10.1002/2015EA000107
Westerink, J. J., Luettich, R. A., Baptists, A. M., Scheffner, N. W., & Farrar, P. (1992). Tide and storm surge predictions using finite element model. *Journal of Hydraulic Engineering*, *118*(10), 1373–1390. https://doi.org/10.1061/(ASCE)0733-9429(1992)118:10(1373)
Westerink, J. J., Luettich, R. A., & Muccino, J. C. (1994). Modelling tides in the western North Atlantic using unstructured graded grids. *Tellus A*, *46*(2), 178–199. https://doi.org/10.1034/j.1600-0870.1994.00007.x
Williams, D. M., & Erikson, L. H. (2021). Knowledge gaps update to the 2019 IPCC special report on the ocean and cryosphere: Prospects to refine coastal flood hazard assessments and adaptation strategies with at-risk communities of Alaska. *Frontiers in Climate*, *3*, 1–11. https://doi.org/10.3389/fclim.2021.761439
Williams, T. D., Bennetts, L. G., Squire, V. A., Dumont, D., & Bertino, L. (2013). Wave–ice interactions in the marginal ice zone. Part 1: Theoretical foundations. *Ocean Modelling*, *71*, 81–91. https://doi.org/10.1016/j.ocemod.2013.05.010
Yang, C.-Y., Liu, J., & Chen, D. (2024). Understanding the influence of ocean waves on Arctic sea ice simulation: A modeling study with an atmosphere–ocean–wave–sea ice coupled model. *The Cryosphere*, *18*(3), 1215–1239. https://doi.org/10.5194/tc-18-1215-2024
Yu, J., Rogers, W. E., & Wang, D. W. (2022). A new method for parameterization of wave dissipation by sea ice. *Cold Regions Science and Technology*, *199*, 103582. https://doi.org/10.1016/j.coldregions.2022.103582
Zhang, J. (2021). Sea ice properties in high-resolution sea ice models. *Journal of Geophysical Research: Oceans*, *126*(1), 1–15. https://doi.org/10.1029/2020JC016686